THE CALIFORNIA PLANET SURVEY. I. FOUR NEW GIANT EXOPLANETS[*]

Andrew W. Howard[1,2,11], John Asher Johnson[3], Geoffrey W. Marcy[1], Debra A. Fischer[4], Jason T. Wright[5],
David Bernat[5], Gregory W. Henry[6], Kathryn M. G. Peek[1], Howard Isaacson[4], Kevin Apps[7], Michael Endl[8],
William D. Cochran[8], Jeff A. Valenti[9], Jay Anderson[9], and Nikolai E. Piskunov[10]

[1] Department of Astronomy, University of California, Berkeley, CA 94720-3411, USA
[2] Space Sciences Laboratory, University of California, Berkeley, CA 94720-7450, USA; howard@astro.berkeley.edu
[3] Department of Astrophysics, California Institute of Technology, MC 249-17, Pasadena, CA 91125, USA
[4] Department of Astronomy, Yale University, New Haven, CT 06511, USA
[5] The Pennsylvania State University, University Park, PA 16802, USA
[6] Center of Excellence in Information Systems, Tennessee State University, 3500 John A. Merritt Blvd., Box 9501, Nashville, TN 37209, USA
[7] 75B Cheyne Walk, Horley, Surrey RH6 7LR, UK
[8] McDonald Observatory, University of Texas at Austin, Austin, TX 78712, USA
[9] Space Telescope Science Institute, 3700 San Martin Dr., Baltimore, MD 21218, USA
[10] Department of Astronomy and Space Physics, Uppsala University, Box 515, 751 20 Uppsala, Sweden

ABSTRACT

We present precise Doppler measurements of four stars obtained during the past decade at Keck Observatory by the California Planet Survey (CPS). These stars, namely, HD 34445, HD 126614, HD 13931, and Gl 179, all show evidence for a single planet in Keplerian motion. We also present Doppler measurements from the Hobby-Eberly Telescope (HET) for two of the stars, HD 34445 and Gl 179, that confirm the Keck detections and significantly refine the orbital parameters. These planets add to the statistical properties of giant planets orbiting near or beyond the ice line, and merit follow-up by astrometry, imaging, and space-borne spectroscopy. Their orbital parameters span wide ranges of planetary minimum mass ($M \sin i = 0.38$–$1.9\ M_{\rm Jup}$), orbital period ($P = 2.87$–11.5 yr), semimajor axis ($a = 2.1$–5.2 AU), and eccentricity ($e = 0.02$–0.41). HD 34445 b ($P = 2.87$ yr, $M \sin i = 0.79\ M_{\rm Jup}$, $e = 0.27$) is a massive planet orbiting an old, G-type star. We announce a planet, HD 126614 Ab, and an M dwarf, HD 126614 B, orbiting the metal-rich star HD 126614 (which we now refer to as HD 126614 A). The planet, HD 126614 Ab, has minimum mass $M \sin i = 0.38\ M_{\rm Jup}$ and orbits the stellar primary with period $P = 3.41$ yr and orbital separation $a = 2.3$ AU. The faint M dwarf companion, HD 126614 B, is separated from the stellar primary by 489 mas (33 AU) and was discovered with direct observations using adaptive optics and the PHARO camera at Palomar Observatory. The stellar primary in this new system, HD 126614 A, has the highest measured metallicity ([Fe/H] = +0.56) of any known planet-bearing star. HD 13931 b ($P = 11.5$ yr, $M \sin i = 1.88\ M_{\rm Jup}$, $e = 0.02$) is a Jupiter analog orbiting a near solar twin. Gl 179 b ($P = 6.3$ yr, $M \sin i = 0.82\ M_{\rm Jup}$, $e = 0.21$) is a massive planet orbiting a faint M dwarf. The high metallicity of Gl 179 is consistent with the planet–metallicity correlation among M dwarfs, as documented recently by Johnson & Apps.

Key words: binaries: visual – planetary systems – stars: individual (HD 34445, HD 126614, HD 24496, HD 13931, G1 179) – techniques: high angular resolution – techniques: photometric – techniques: radial velocities

1. INTRODUCTION

The distributions of the masses and orbits of Jovian-mass exoplanets offer key tests of planet formation theory. Most theories predict that giant planets form beyond the "snow line" and migrate inward on a time scale that competes with the lifetime of the protoplanetary disk (Thommes et al. 2008; Ida & Lin 2008; Rice & Armitage 2005; Alibert et al. 2005; Trilling et al. 2002). Among various theories for formation, core accretion has been shown efficient at producing, within ∼3 Myr, planets of Neptune to Jupiter mass, orbiting within 5 AU (Benz et al. 2008; Dodson-Robinson et al. 2008).

These models of giant planet formation and orbital evolution may be directly tested against observations of giant planets found by the Doppler method. The models predict a clearing of gaps in the protoplanetary disks, establishing the distribution of planet masses, allowing a direct comparison with Doppler observed minimum masses ($M \sin i$). According to the models, the disk dissipates after the planets have undergone some inward migration, leaving them at their current orbital distances. The resulting predicted distribution of semimajor axes can be compared with the observed orbits of giant planets. There remains potential value in both enhancing the sophistication of planet formation theory and in observing a large enough statistical sample of giant planets to permit robust and informative tests of the theory. Moreover, planet–planet interactions among giant planets must be predicted and compared with the distributions of orbital elements (especially eccentricity) for systems containing multiple giant planets, e.g., Wright et al. (2009); Ford & Chiang (2007); Ford & Rasio (2008); Jurić & Tremaine (2008). Giant planets also gravitationally interact with the dust in their planetary system to shape, on time scales of only years, the dust evolution of the planetary system (Lisse et al. 2007; Beichman et al. 2007; Payne et al. 2009).

As of 2009 May, 350 exoplanets have been discovered, with remarkable properties including close-in orbits, large

orbital eccentricities, multi-planet systems, and orbital resonances (Mayor & Udry 2008; Marcy et al. 2008). The hot Jupiters have received the most attention, observationally and theoretically, yielding extraordinary information about their chemical composition, internal structure, and atmospheric behavior. However, most known gas giant planets orbit beyond 1 AU, realizing the population that formed beyond the ice line as predicted by theory, and as seen in our solar system.

In 1997, we began a Doppler search for giant planets in Jovian orbits at Keck Observatory. We monitor over 1800 stars within 50 pc, with special attention given to those within 20 pc. We have acquired a Doppler time baseline of well over 8 yr for nearly all of them. The detected long-period exoplanets reveal the distribution of their masses, semimajor axes, and orbital eccentricities for the general population of planetary systems. Remarkably, the exoplanets exhibit a sharp rise in occurrence beyond 1 AU (Johnson et al. 2007b; Cumming et al. 2008), indicating that a great population of giant planets resides there. Many of these planets remain undiscovered even after 10 yr of Doppler monitoring, as the amplitudes of a few meters per second require high Doppler precision and a clear indication of Keplerian motion, which is challenging for orbital periods comparable to the duration of observations. Nonetheless, the analysis of Doppler completeness shows that 15%–18% of all nearby stars have giant planets between 3 and 20 AU (Cumming et al. 2008). Surely, these giant planets offer strong statistical information on the formation and subsequent dynamical evolution of gas giants in general.

Unfortunately, with only a decade of Doppler data orbits beyond 4 AU are just coming into our Doppler field of view. The recently announced Jupiter-analog orbiting HD 154345 with $a = 5.0$ AU (and a circular orbit) exhibited nearly one full orbital period only after 10 full years of Doppler data were collected (Wright et al. 2008). But the number of giant planets known for orbiting beyond 1 AU remains so small that extraordinary statistical efforts are required to extrapolate the true underlying properties (Cumming et al. 2008). Thus, there remains a need for enlarging the observed population of giant planets, especially with the prospect of follow-up observations by such instruments as the *James Webb Space Telescope* (*JWST*), the Gemini Planet Imager (GPI), and the Spectro-Polarimetric High-contrast Exoplanet Research (SPHERE) instrument for the Very Large Telescope (VLT).

In the future, knowledge of giant planets around the nearest stars will be crucial for detecting Earth-sized planets, e.g., by the Space Interferometry Mission (SIM; Unwin et al. 2008), as the giant planets add a "noise" to the astrometric signal (Traub et al. 2009). One concern is that multiple giant planets orbiting beyond 2 AU will cause curved astrometric motion, with the linear part being (erroneously) absorbed into the inferred proper motion. The resulting residuals will have a time scale of ∼1 yr, constituting an astrophysical "noise," compromising the detection of the terrestrial planets. Thus, future astrometric missions will benefit greatly from ∼15 yr of radial velocity (RV) data. The characterization of both giant and rocky planets will be important for future missions that image and take spectra of planets, such as the Terrestrial Planet Finder and Darwin (Kaltenegger et al. 2006; Lawson et al. 2008). As a result, we continue to survey nearby stars that are likely targets for such surveys (Kaltenegger et al. 2010). Here, we describe Doppler measurements from Keck Observatory and from the Hobby-Eberly Telescope (HET) for four stars that shows signs of harboring a planet beyond 1 AU.

2. STELLAR SAMPLE AND PROPERTIES

Among the 1800 FGKM stars we monitor at the Keck telescope for giant planets, 1330 of them have been monitored from 1997 to the present with a precision of 1–3 m s^{-1}. The sample contains a nearly volume-limited sample of stars within five bins of $B - V$ color, between 0.60 and 1.5. It is nearly devoid of both binary stars separated by less than $2''$ due to mutual contamination at the slit of the spectrometer and magnetically active stars younger than 1 Gyr due to their excessive velocity "jitter" (Wright 2005). The complete list of target stars is given in Wright et al. (2004) including the stars that do not have detected planets, permitting statistical analyses of the frequency of planets, e.g., Johnson et al. (2007a); Cumming et al. (2008); Butler et al. (2006).

Only 7% of our stars surveyed for a decade reveal clear Keplerian Doppler variations at a 3σ limit of 10 m s^{-1}. However, Cumming et al. (2008) accounted for incompleteness in our Doppler survey and predicted that ∼18% of FGK stars harbor a gas giant of Saturn mass or above within 20 AU. This prediction suggests that another 11% of our target stars harbor giant planets yet to be revealed, with continued monitoring. The four stars presented here presumably harbor some of these giant planets by predicted Cumming et al. (2008).

We measure atmospheric parameters of the target stars by LTE spectroscopic analysis of our Keck/HIRES spectra using the Spectroscopy Made Easy ("SME") code (Valenti & Piskunov 1996) as implemented by Valenti & Fischer (2005) and Fischer & Valenti (2005). The analysis yields a best-fit estimate of $T_{\rm eff}$, log g, [Fe/H], $v \sin i$. We could not carry out an LTE analysis of Gl 179 because its cool temperature resides outside the lowest temperature for which our continuous and molecular opacities are accurate.

The luminosity of each star is determined from the apparent V-band magnitude, the bolometric correction, and the parallax from Hipparcos. From $T_{\rm eff}$ and the luminosity, we determine the stellar mass, radius, and an age estimate by associating those observed properties with a model from the stellar interior calculations of Takeda et al. (2007, 2008). These properties, along with parallaxes and implied distances from the van Leeuwen (2007) reduction of Hipparcos data, are tabulated in Table 1.

Since Gl 179 is faint and cool, we could not use SME or the Takeda et al.'s stellar interior models to compute stellar properties. Instead, we used a variety of other techniques to estimate the properties listed in Table 1. We determined the mass of Gl 179 by using the mass-luminosity calibration of Delfosse et al. (2000), applying its apparent K-band magnitude, $K = 6.942$, and parallax of 81.4 mas. The resulting mass is $M_\star = 0.357 \pm 0.030\ M_\odot$, with the uncertainty from the scatter in best-fit M–L relation. Johnson & Apps (2009) estimate a metallicity of [Fe/H] $= 0.30 \pm 0.10$ for Gl 179 based on its absolute K-band magnitude, M_K, and $V - K$ color. We estimate $L_\star = 0.016 \pm 0.002\ L_\odot$ from the bolometric correction, $T_{\rm eff} = 3370 \pm 100$ K from Bessell (1995), $R_\star = 0.38 \pm 0.02\ R_\odot$ from the Stefan–Boltzmann law, $v \sin i < 1.5$ km s^{-1} from visual inspection of the Gl 179 spectrum (Figure 1), and log $g = 4.83$ from the stellar mass and radius.

We also measure the chromospheric emission in the Ca II H & K line cores, providing $S_{\rm HK}$ values (Isaacson 2009; Wright et al. 2004) on the Mt. Wilson system. For each star, the time series Keck RVs and $S_{\rm HK}$ values are uncorrelated (as measured by a Pearson correlation coefficient). We converted the average

Table 1
Stellar Properties

| Parameter	HD 34445	HD 126614 A	HD 13931	Gl 179
Spectral type	G0 V	K0 V	G0 V	M3.5 V
M_V	4.04 ± 0.10	4.64 ± 0.17	4.32 ± 0.10	11.5 ± 0.11
$B - V$	0.661 ± 0.015	0.810 ± 0.004	0.642 ± 0.015	1.590 ± 0.015
V	7.31 ± 0.03	8.81 ± 0.002	7.61 ± 0.03	11.96 ± 0.03
Parallax (mas)	21.5 ± 0.7	13.8 ± 1.0	22.6 ± 0.7	81.4 ± 4.0
Distance (pc)	46.5 ± 1.5	72.4 ± 5.3	44.2 ± 1.4	12.3 ± 0.6
[Fe/H]	$+0.14 \pm 0.04$	$+0.56 \pm 0.04$	$+0.03 \pm 0.04$	$+0.30 \pm 0.10$
$T_{\rm eff}$ (K)	5836 ± 44	5585 ± 44	5829 ± 44	3370 ± 100
$v \sin i$ (km s^{-1})	2.7 ± 0.5	2.0 ± 0.5	2.0 ± 0.5	<1.5
$\log g$	4.21 ± 0.08	4.39 ± 0.08	4.30 ± 0.08	4.83
$L_\star$ ($L_\odot$)	2.01 ± 0.2	1.21 ± 0.19	1.57 ± 0.14	0.016 ± 0.02
$M_\star$ ($M_\odot$)	1.07 ± 0.02	1.145 ± 0.03	1.022 ± 0.02	0.357 ± 0.03
$R_\star$ ($R_\odot$)	1.38 ± 0.08	1.09 ± 0.06	1.23 ± 0.06	0.38 ± 0.02
Age (Gyr)	8.5 ± 2.0	7.2 ± 2.0	8.4 ± 2.0	$\ldots$
$S_{\rm HK}$	0.148	0.152	0.161	0.956
$\log R'_{\rm HK}$	-5.07	-5.44	-4.99	-5.20
$P_{\rm rot}$ (days)	~ 22	~ 99	~ 26	$\ldots$
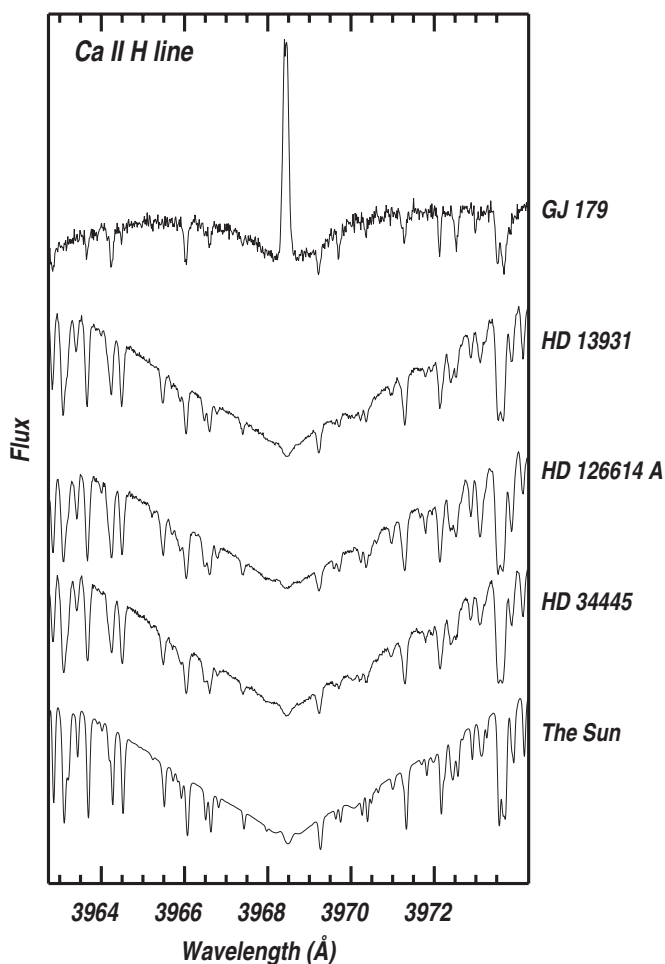
Figure 1. Spectra near the Ca II H line for all four stars discussed here. The emission reversals reflect magnetic activity on stars that correlates with photospheric velocity jitter. The resulting chromospheric cooling rate, measured as a fraction of stellar luminosity, $\log R'_{\rm HK}$, is listed in Table 1. The inferred values of jitter are listed in Table 3.

$S_{\rm HK}$ values for each star to $\log R'_{\rm HK}$ as per Noyes et al. (1984), providing an estimate of the age and rotation period of the stars. The $\log R'_{\rm HK}$ relation is not calibrated for cool M stars, but we include the computed value for Gl 179 nonetheless. All of the

resulting stellar parameters are reported in Table 1. We discuss the salient properties of each star in Sections 5–8.

HD 126614 is a binary star system composed of a bright primary, HD 126614 A, and a faint M dwarf companion, HD 126614 B, separated by $\sim0\rlap{.}''5$. The heretofore unknown companion is significantly fainter ($\Delta V = 7.8$ mag) and did not significantly contaminate the spectroscopic or photometric observations. (See Section 6 for details.)

3. PHOTOMETRIC OBSERVATIONS FROM THE FAIRBORN OBSERVATORY

We have obtained between two and seven years of high-precision differential photometry of all target stars in this paper with the exception of Gl 179. The observations were acquired with the T12 0.8 m automatic photometric telescope (APT) at the Fairborn Observatory. This APT can detect short-term, low-amplitude brightness variability in solar-type stars due to rotational modulation in the visibility of photospheric starspots (e.g., Henry et al. 1995) as well as longer-term variations associated with stellar magnetic cycles (Henry 1999). Therefore, photometric observations can help to establish whether observed RV variations in a star are due to reflex motion caused by a planetary companion or due to the effects of stellar activity (e.g., Queloz et al. 2001; Paulson et al. 2004). Photometric observations can also lead to the detection of planetary transits and the direct determination of planetary radii, as in Winn et al. (2008).

We acquired 854 nightly photometric observations of the three planetary host stars between 2000 November and 2009 March. HD 13931, HD 34445, and HD 126614 A were observed by the T12 APT, a functional duplicate of the T8 0.8 m APT and two-channel photometer described in Henry (1999). All target stars were observed differentially with respect to two comparison stars in the Strömgren b and y bands. One to four observations per night were made of each target, depending on the seasonal visibility of each star. To increase our photometric precision, we averaged the individual b and y differential magnitudes into a composite $(b + y)/2$ passband. Stars fainter than $V = 8$ were observed for 90 s per observation, while brighter stars were observed for 60 s.

The results of our APT observations are summarized in Table 2, which identifies the comparison stars used, the number and timespan of the observations, and our measures of brightness

Table 2
Summary of Photometric Observations from Fairborn Observatory

Target Star (1)	Comparison Star 1 (2)	Comparison Star 2 (3)	N_{obs} (4)	N_{yrs} (5)	Date Range (JD−2,400,000) (6)	Target σ_{short} (mag) (7)	Comp σ_{short} (mag) (8)	Target σ_{long} (mag) (9)	Comp σ_{long} (mag) (10)
HD 34445	HD 34907	HD 35241	560	7	52591–54913	0.00155	0.00156	0.00102	0.00120
HD 126614	HD 127265	HD 124988	113	2	54171–54634	0.00158	0.00163	0.00002	0.00161
HD 13931	HD 13024	HD 14064	181	2	54730–54532	0.00153	0.00164	0.00158	0.00060

Table 3
Single Planet Keplerian Orbital Solutions

Parameter	HD 34445	HD 126614 A	HD 13931	Gl 179
P (yr)	2.87 ± 0.03	3.41 ± 0.05	11.5 ± 1.1	6.26 ± 0.16
P (days)	1049 ± 11	1244 ± 17	4218 ± 388	2288 ± 59
e	0.27 ± 0.07	0.41 ± 0.10	0.02 ± 0.05	0.21 ± 0.08
K (m s^{-1})	15.7 ± 1.4	7.3 ± 0.7	23.3 ± 1.4	25.8 ± 2.2
T_p (JD − 2,440,000)	$13,781 \pm 48$	$13,808 \pm 52$	$14,494 \pm 904$	$15,140 \pm 104$
ω (deg)	104 ± 19	243 ± 19	290 ± 78	153 ± 24
dv/dt (m s^{-1} yr^{-1})	$\equiv 0.0$	16.2 ± 0.2	$\equiv 0.0$	$\equiv 0.0$
$M \sin i$ (M_{Jup})	0.79 ± 0.07	0.38 ± 0.04	1.88 ± 0.15	0.82 ± 0.07
a (AU)	2.07 ± 0.02	2.35 ± 0.02	5.15 ± 0.29	2.41 ± 0.04
N_{obs} (Keck, binned)	68	70	39	30
N_{obs} (HET, binned)	50	. . .	. . .	14
Median binned uncertainty (Keck, m s^{-1})	1.4	1.3	1.3	4.7
Median binned uncertainty (HET, m s^{-1})	2.7	. . .	. . .	7.2
Assumed Keck pre-upgrade jitter (m s^{-1})	3.0	3.0	3.0	3.0
Assumed Keck post-upgrade jitter (m s^{-1})	2.0	2.0	2.0	2.5
Assumed HET jitter (m s^{-1})	2.0	. . .	. . .	2.5
rms to fit (m s^{-1})	7.31	3.99	3.31	9.51
$\sqrt{\chi_\nu^2}$	2.39	1.42	1.01	1.78

variability in the target and comparison stars. All three of the observed stars have very little chromospheric activity (Table 1 and Figure 1). Therefore, given the well-known connection between chromospheric activity and brightness variability in solar-type stars (see, e.g., Henry 1999, Figure 11), we did not expect to find significant photometric variability in these four targets.

We use the standard deviation as a simple metric for brightness variability of our target and comparison stars, and we measure the variability on both night-to-night (σ_{short}) and year-to-year (σ_{long}) time scales. In general, the standard deviations of individual measurements of pairs of constant stars fall in the range 0.0012–0.0017 mag for these telescopes. Column 7 of Table 2 gives the standard deviation of the individual target minus comparison star differential magnitudes averaged across both comparison stars and across all observing seasons. Column 8 gives the standard deviation of the individual differential magnitudes between the two comparison stars averaged across all observing seasons. We compute the (σ_{long}) values in the same manner but with the yearly mean differential magnitudes rather than individual nightly magnitudes. The photometric results for each of the four stars are briefly discussed in the following sections. Given the moderately long orbital periods and the current uncertainties in the orbital parameters (Table 3), a search for planetary transits in any of the four target stars is impractical.

4. SPECTROSCOPIC OBSERVATIONS AND KEPLERIAN ORBITAL SOLUTIONS

4.1. Keck Observations and Doppler Reduction

We observed HD 34445, HD 126614 A, HD 13931, and Gl 179 using the HIRES echelle spectrometer (Vogt et al. 1994)

on the 10 m Keck I telescope. These stars were each observed 30–70 times each over 10–12 yr. Typical exposure times for these stars were 100, 357, 130, and 500 s, respectively. All observations were made with an iodine cell mounted directly in front of the spectrometer entrance slit. The dense set of molecular absorption lines imprinted on the stellar spectra provide a robust wavelength fiducial against which Doppler shifts are measured, as well as strong constraints on the shape of the spectrometer instrumental profile at the time of each observation (Marcy & Butler 1992; Valenti et al. 1995).

We measured the Doppler shift from each star-times-iodine spectrum using a modeling procedure modified from the method described by Butler et al. (1996). The most significant modification is the way we model the intrinsic stellar spectrum, which serves as a reference point for the relative Doppler shift measurements for each observation. Butler et al. use a version of the Jansson (1995) deconvolution algorithm to remove the spectrometer's instrumental profile from an iodine-free template spectrum. We instead use a new deconvolution algorithm developed by one of us (J.A.J.) that employs a more effective regularization scheme, which results in significantly less noise amplification and improved Doppler precision.

Figure 2 shows the RV time series for four stable stars with characteristics similar to the planet-bearing stars presented herein, demonstrating our measurement precision over the past decade on a variety of spectral types. In 2004 August, the Keck HIRES spectrometer was upgraded with a new detector. The previous 2K × 2K pixel Tektronix CCD was replaced by an array of three 4K × 2K pixel MIT-LL CCDs. The new detector produces significantly higher velocity precision due to its improved charge transfer efficiency and charge diffusion characteristics, smaller pixels (15 μm versus 24 μm), higher quantum efficiency, increased spectral coverage, and lower
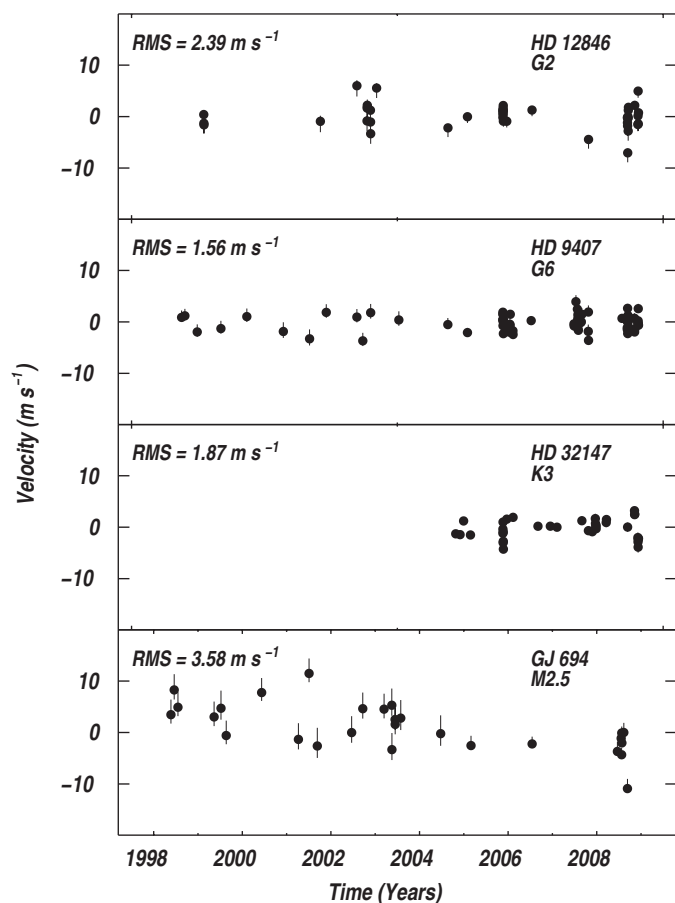
Figure 2. Radial velocity time series for four stable stars in our Keck Doppler survey. These stars demonstrate long-term velocity stability over a wide range of spectral types. Gl 694 (M2.5, V = 10.5) shows that our velocity precision is reduced around faint, late spectral type stars, but that it is sufficient to detect the planet around Gl 179 (M3.5, V = 11.96). The binned velocities with measurement uncertainties (but not jitter) are plotted. Panels are labeled with star name, spectral type, and rms to a linear fit.

read noise. Our post-upgrade measurements exhibit a typical long-term rms scatter of ~1.5 m s^{-1} for bright, quiescent stars, compared to ~2.5 m s^{-1} for pre-upgrade measurements. (Measurements prior to JD 2,453,237 are pre-upgrade.) The pre- and post-upgrade measurements also lack a common velocity zero point, but we fit for and corrected this offset to within ~2 m s^{-1} for every star observed at Keck using a large set of stable stars with many pre- and post-upgrade observations. To further limit the impact of the velocity discontinuity, we let the offset float in the Keplerian fits below, effectively treating pre-upgrade and post-upgrade observations as coming from two different telescopes (except for HD 13931, which does not have enough post-upgrade measurements to allow for a floating offset).

With the exception of Gl 179, these planet-bearing stars are bright G and K stars, and the Keck RVs have median single measurement uncertainties of 1.2–1.4 m s^{-1}. In some instances, we made two or more consecutive observations of the same star and binned the velocities in 2 hr time bins, thereby reducing the associated measurement uncertainties. Gl 179 is substantially fainter (V = 11.96), and its median measurement uncertainty of 4.2 m s^{-1} is dominated by Poisson noise from photon statistics. For each of these stars, the measurement uncertainty is the weighted standard deviation of the mean of the velocity

measured from each of the ~700 2 Å chunks in the echelle spectrum (Butler et al. 1996).

4.2. HET Observations and Doppler Reduction

We observed two of the stars, HD 34445 and Gl 179, with the HET (Ramsey et al. 1998) at the McDonald Observatory, as part of the ongoing Doppler surveys of FGK-type stars (Cochran et al. 2004) and M dwarfs (Endl et al. 2003). We use the High-Resolution-Spectrograph (HRS; Tull 1998) in combination with an I$_2$-cell at a resolving power of $R = 60,000$ to measure precise RVs. The observing strategy and data reduction pipeline are detailed in Cochran et al. (2004) and a description of our I$_2$-data modeling code "Austral" can be found in Endl et al. (2000).

HET observations of HD 34445 begun in 2003 October and we collected a total of 50 HRS spectra since then. We started RV monitoring of Gl 179 a year later, in 2004 October, and so far we have obtained 13 spectra of this faint M dwarf.

4.3. Keplerian Models

For each of the four stars below, we present a single-planet Keplerian fit to the measured velocities. For HD 126614 A, we add a linear velocity trend to the model. Table 3 summarizes the observing statistics, best-fit Keplerian orbital parameters, and measures of the goodness-of-fit for these planets. In this subsection, we describe the Keplerian modeling and related topics associated for all of the stars. We discuss the planet-bearing stars individually in Sections 5–8.

With the measured velocities for each star we performed a thorough search of the orbital parameter space for the best-fit, single-planet Keplerian orbital model using the partially lin-earized, least-squares fitting procedure described in Wright & Howard (2009). Each velocity measurement was assigned a weight, w, constructed from the quadrature sum of the mea-surement uncertainty (σ_{RV}) and a jitter term (σ_{jitter}), i.e., $w = 1/(\sigma_{RV}^2 + \sigma_{jitter}^2)$. Following Wright (2005), and based on the val-ues of S_{HK}, M_V, and $B - V$, we estimate σ_{jitter} for each of the stars (Table 3). These empirical estimates account for RV variabil-ity due to myriad sources of stellar noise, including the ve-locity fields of magnetically controlled photospheric turbu-lence (granulation, super-granulation, and meso-granulation), rotational modulation of stellar surface features, stellar pulsa-tion, and magnetic cycles, as well as undetected planets and uncorrected systematic errors in the velocity reduction (Saar et al. 1998; Wright 2005). We adopt larger values of jitter for pre-upgrade Keck measurements ($\sigma_{jitter} = 3$ m s^{-1}) than for HET measurements and post-upgrade Keck measurements ($\sigma_{jitter} = 2$–2.5 m s^{-1}). The difference accounts for the slightly larger systematic errors incurred in the reduction of pre-upgrade spectra.

The Keplerian parameter uncertainties for each planet were derived using a Monte Carlo method (Marcy et al. 2005) and do not account for correlations between parameter errors.

For stars with small Doppler amplitudes (HD 34445 and HD 126614 A), we also explicitly considered the null hypoth-esis—that the velocity periodicity represented by the Keplerian orbital fit arose from chance fluctuations in the velocities—by calculating a false alarm probability (FAP) based on $\Delta\chi^2$, the goodness-of-fit statistic (Howard et al. 2009; Marcy et al. 2005; Cumming et al. 2008). These FAPs compare the measured data to 1000 scrambled data sets drawn randomly with replacement from the original measurements. (The linear velocity trend seen

in HD 126614 A was subtracted from the velocities before scrambling.) For each data set, we compare a best-fit Keplerian model to the null hypothesis (a linear fit to the data) by computing $\Delta\chi^2 = \chi^2_{\rm lin} - \chi^2_{\rm Kep}$, where $\chi^2_{\rm lin}$ and $\chi^2_{\rm Kep}$ are the values of χ^2 for linear and Keplerian fits to the data, respectively. The $\Delta\chi^2$ statistic measures the improvement in the fit of a Keplerian model compared to a linear model of the same data. The FAP is the fraction of scrambled data sets that have a larger value of $\Delta\chi^2$ than for the unscrambled data set. That is, the FAP measures the fraction of scrambled data sets where the statistical improvement from a best-fit Keplerian model over a linear model is greater than the statistical improvement of a Keplerian model over a linear model for the actual measured velocities. We use $\Delta\chi^2$ as the goodness-of-fit statistic, instead of other measures such as χ_ν for a Keplerian fit, to account for the fact that the scrambled data sets, drawn from the original velocities *with replacement*, have different variances, which sometimes artificially improve the fit quality (i.e., some scrambled data sets contain fewer outlier velocities and have lower rms). It is important to note that this FAP does not measure the probability of non-planetary sources of true velocity variation masquerading as a planetary signature.

5. HD 34445

5.1. Stellar Characteristics

HD 34445 (= HIP 24681) is spectral type G0 V, with $V = 7.31$, $B - V = 0.66$, and $M_V = 4.04$, placing it ∼0.8 mag above the main sequence as defined by Wright (2005). It is chromospherically quiet with $S_{\rm HK} = 0.15$ and $\log R'_{\rm HK} = -5.07$ (Isaacson 2009), implying a rotation period of ∼22 days (Noyes et al. 1984). Valenti & Fischer (2005) measured a super-solar metallicity of [Fe/H] = +0.14 using SME. Its placement above the main-sequence and low chromospheric activity are consistent with an old, quiescent star of age 8.5 ± 2 Gyr.

5.2. Photometry from Fairborn Observatory

We have 560 individual photometric observations of HD 34445 spanning seven consecutive observing seasons. The mean short-term standard deviation of HD 34445 is comparable to the mean standard deviations of the comparison stars (Table 2; Columns 7 and 8); both are within the range of our typical measurement precision for single observations. We performed periodogram analyses over the range of 1–100 days on the seven individual observing seasons and on the entire data sets and found no significant periodicity in either HD 34445 or the comparison stars. Therefore, our short-term variability measurements of 0.00155 and 0.00156 mag are upper limits to any real nightly brightness variability in the target and comparison stars.

Similarly, the long-term standard deviations of HD 34445 and the comparison stars are similar (Table 2; Columns 9 and 10), indicating that we have not resolved any intrinsic year-to-year variability in HD 34445. Henry (1999) and Wright et al. (2008) present data sets that have seasonal means with standard deviations as low as 0.0002 mag, which we take as our measurement precision for seasonal mean magnitudes. Thus, our non-detection of long-term variability in HD 34445 may be compromised by low-level variability in one or both of the comparison stars.
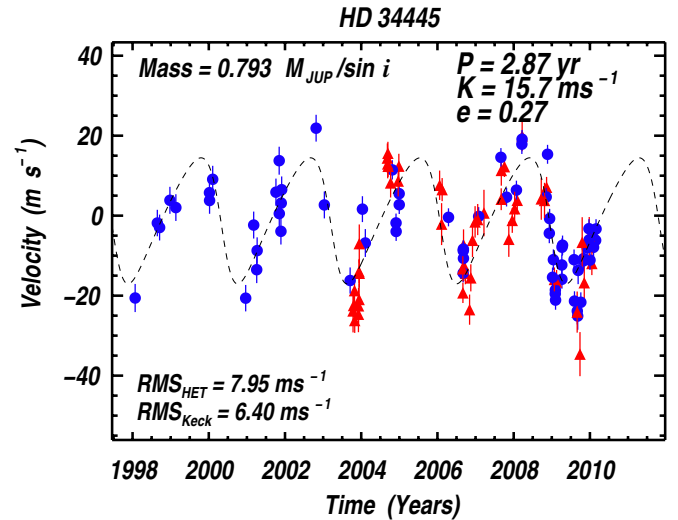

Figure 3. Measured velocity vs. time for HD 34445 with the associated best-fit Keplerian model (dashed line). Filled blue circles represent measurements from Keck, while filled red triangles represent HET measurements. The error bars show the quadrature sum of measurement uncertainties and jitter.

5.3. Doppler Observations and Keplerian Fit

We monitored the RV of HD 34445 at Keck for the past 12 yr and at the HET for the past 6 yr. Table 4 gives the Julian Dates of the observations, the measured (relative) RVs, the associated measurement uncertainties (excluding jitter), and the telescope used. The 118 velocities listed in Table 4 have an rms of 12.0 m s^{-1} and are plotted as a time series in Figure 3 along with the best-fit, single-planet Keplerian model.

The velocities plotted in Figure 3 reveal a ∼2.8 yr periodicity that is apparent by visual inspection. We searched periods near 2.8 yr, and a wide variety of other periods, to find a single-planet Keplerian model with best-fit parameters, $P = 2.87 \pm 0.03$ yr, $e = 0.27 \pm 0.07$, and $K = 15.7 \pm 1.4$ m s^{-1}, implying a planet of minimum mass $M \sin i = 0.79\ M_{\rm Jup}$ orbiting with semimajor axis $a = 2.07$ AU. The full set of orbital parameters is listed in Table 3.[12] This joint fit has an rms of 7.31 m s^{-1} with $\chi_\nu = 2.39$. The planetary signal was detected in the Keck and HET data sets individually, which have an rms of 6.39 m s^{-1} and 7.95 m s^{-1} about the joint fit, respectively.

We also considered the null hypothesis—that the observed RV measurements are the chance arrangement of random velocities masquerading as a coherent signal—by calculating an FAP. As described in Section 4.3, we computed the improvement in $\Delta\chi^2$ from a constant velocity model to a Keplerian model (without a trend) for 10^3 scrambled data sets. We found that no scrambled data set had a larger value for $\Delta\chi^2$ than for the measured velocities, implying an FAP of less than ∼0.001 for this scenario.

While the single-planet model appears secure, the rms of the velocity residuals (6–8 m s^{-1}) is a factor of ∼2 higher than expected based on the measurement uncertainties and jitter. Two possible explanations for this excess variability are underestimated jitter and additional planets. Jitter seems an unlikely explanation given this star's metallicity, color, and modest evolution. As a comparison, the five stars most similar to HD 34445 ($B - V$ and M_V within 0.05 mag) with 10 or more

---

[11] Advanced mention of the existence of this planet for HD 34445 was made in Fischer & Valenti (2005).

Table 4
Radial Velocities of HD 34445

JD−2440000	Radial Velocity (m s^{-1})	Uncertainty (m s^{-1})	Telescope
10838.76212	−20.59	1.83	K
11051.10569	−1.84	1.40	K
11073.04246	−2.97	1.21	K
11171.84795	3.84	1.55	K
11228.80594	2.02	1.47	K
11550.88478	5.75	1.35	K
11551.88096	3.79	1.43	K
11581.87017	9.09	1.54	K
11898.03487	−20.63	1.39	K
11974.76461	−2.35	1.53	K
12003.74221	−13.51	1.50	K
12007.72006	−8.73	1.41	K
12188.14432	5.87	1.59	K
12219.15109	13.75	1.79	K
12220.08113	0.52	1.80	K
12235.86269	−3.92	1.38	K
12238.88934	3.14	1.61	K
12242.92553	6.49	1.39	K
12572.99576	21.87	1.50	K
12651.93917	2.68	1.53	K
12899.09825	−16.22	1.29	K
12926.86832	−23.82	4.99	H
12932.00108	−22.46	2.09	H
12940.99257	−18.74	3.23	H
12942.98461	−26.21	2.37	H
12978.73611	−24.64	4.03	H
12979.73953	−22.54	4.01	H
12983.88276	−13.97	2.21	H
12984.88936	−20.95	3.41	H
12986.73101	−6.99	4.35	H
12986.86187	−14.40	2.99	H
13016.88898	1.63	1.21	K
13044.79245	−6.83	1.78	K
13255.96162	14.40	3.08	H
13258.95666	12.95	3.01	H
13260.96242	15.60	2.06	H
13262.94700	12.35	1.76	H
13286.88668	8.19	3.05	H
13303.12110	11.45	1.35	K
13338.90162	−1.81	1.21	K
13340.02404	−3.95	1.26	K
13359.69356	8.66	3.28	H
13365.68179	12.38	2.36	H
13368.95279	5.50	1.16	K
13369.80021	2.74	1.19	K
13756.75932	7.60	3.08	H
13775.69673	−2.11	4.85	H
13780.69018	6.51	2.08	H
13841.76181	−0.41	1.05	K
13978.97450	−13.27	2.42	H
13979.97609	−19.30	1.56	H
13982.10169	−14.37	1.16	K
13983.09819	−8.77	0.73	K
13984.10344	−8.36	0.89	K
13985.04721	−10.67	1.11	K
13985.98820	−7.28	3.29	H
13988.96142	−12.49	3.31	H
14003.92771	−14.39	1.91	H
14043.81148	−23.50	3.20	H
14055.77338	−15.55	2.73	H
14071.89776	−6.16	3.70	H
14096.67373	−1.56	3.40	H
14121.60247	−0.97	3.34	H

Table 4
(Continued)

JD−2440000	Radial Velocity (m s^{-1})	Uncertainty (m s^{-1})	Telescope
14130.87196	−0.18	1.17	K
14181.59907	0.66	5.45	H
14344.11108	14.59	1.16	K
14346.97829	4.11	1.86	H
14347.96596	11.32	3.26	H
14377.89952	12.25	1.64	H
14398.06266	4.62	1.17	K
14419.95414	−5.91	3.91	H
14452.85410	−1.18	2.39	H
14475.63706	1.73	3.76	H
14492.85216	6.39	1.25	K
14500.70733	3.84	2.86	H
14544.81179	17.87	1.41	K
14546.73807	19.12	1.16	K
14547.60716	19.93	3.26	H
14730.92837	4.20	4.83	H
14762.00435	3.81	3.93	H
14777.95271	4.68	1.02	K
14781.79952	7.11	1.62	H
14791.00635	15.34	1.26	K
14807.92630	−4.41	1.46	K
14810.89575	−0.73	1.37	K
14838.84447	−15.41	1.40	K
14846.97512	−11.01	1.61	K
14856.59752	−15.94	2.22	H
14864.89937	−19.53	1.24	K
14865.83319	−18.59	0.96	K
14867.78335	−21.11	1.35	K
14877.68465	−16.60	2.26	H
14927.76208	−12.33	1.36	K
14928.72560	−15.91	1.23	K
14929.73178	−7.89	0.92	K
14934.73601	−7.39	1.36	K
15045.13099	−11.01	1.59	K
15049.12654	−21.37	1.43	K
15074.98600	−24.11	4.74	H
15076.12099	−23.84	2.69	K
15080.13683	−25.10	2.79	K
15084.13106	−13.69	2.79	K
15101.90535	−34.62	5.14	H
15110.12260	−21.65	1.46	K
15123.00538	−6.66	5.95	H
15135.10186	−11.30	1.37	K
15135.95876	−10.74	1.39	K
15142.80591	−16.77	4.28	H
15170.83820	−8.05	1.29	K
15187.83253	−3.26	1.27	K
15189.83159	−6.05	1.37	K
15190.67571	−5.15	4.38	H
15197.82141	−11.12	1.38	K
15215.60340	−11.95	2.12	H
15229.77934	−5.58	1.21	K
15231.95374	−7.91	1.21	K
15251.85907	−6.17	1.43	K
15255.79845	−3.31	1.39	K

Keck observations have velocity rms in the range 2.6–4.9 m s^{-1}. We searched a wide range of possible periods for a second planet and found several candidates, the strongest of which has $P_c = 117$ days, $M_c \sin i = 52\ M_\oplus$, and an FAP of a few percent. A significant number of additional measurements are required to confirm this planet and rule out other periods.

6. HD 126614 A

6.1. Stellar Characteristics

HD 126614 (= HIP 70623) is identified in the Henry Draper and Hipparcos catalogs as a single star. As described in Section 6.5, we directly detected by adaptive optics (AO) a faint M dwarf companion separated by 489 mas from the bright primary. We refer to the bright primary star as HD 126614 A and the faint companion as HD 126614 B. These stars are unresolved in the Doppler and photometric variability observations described below. The planet announced below orbits HD 126614 A and is named HD 126614 Ab. In addition, HD 126614 A is orbited by a second M dwarf, NLTT 37349, in a much wider orbit (Gould & Chanamé 2004). This outer stellar companion is separated from HD 126614 A by 42″ and does not contaminate the Doppler or photometric observations.

HD 126614 A is spectral type K0 V, with $V = 8.81$, $B - V = 0.81$, and $M_V = 4.64$, placing it ∼1.2 mag above the main sequence. It is chromospherically quiet with $S_{HK} = 0.15$ and $\log R'_{HK} = -5.44$ (Isaacson 2009), implying a rotation period of 99 days, which is off the scale of the calibration, but suggests that it is longer than 50 days (Noyes et al. 1984). Valenti & Fischer (2005) measured an extremely high metallicity of [Fe/H] = +0.56 using SME. This is the highest metallicity measured in the 1040 stars in the SPOCS catalog (Valenti & Fischer 2005). The low chromospheric activity ($S_{HK} = 0.15$) is consistent with the age estimate of 7.2 ± 2.0 Gyr from the SME analysis (Valenti & Fischer 2005).

6.2. Photometry from Fairborn Observatory

We have only 113 photometric observations of HD 126614 A covering two observing seasons. Periodogram analyses over the range of 1–100 days found no significant periodicity in either HD 126614 A or its comparison stars. The short-term variability of 0.00158 mag in the target star is comparable to 0.00163 mag in the comparison stars and to our measurement precision. The measurement of long-term variability in HD 126614 A is compromised by low-amplitude variability in one or both comparison stars. Thus, 0.0016 mag serves as an upper limit to both long- and short-term variability in HD 126624 A.

6.3. Doppler Observations and Keplerian Fit

We monitored the RV of HD 126614 A at Keck for the past 11 yr. Table 5 gives the Julian Dates of the observations, the measured (relative) radial velocities, and the associated measurement uncertainties (excluding jitter). The 70 velocities listed in Table 5 and plotted as a time series in Figure 4 display a strong linear trend of 16.2 m s^{-1} yr^{-1} with an rms of 6.6 m s^{-1} about that trend. For clarity, the same velocities are plotted in Figure 5 with the trend subtracted.

After subtracting the linear trend, a Lomb–Scargle periodogram of the HD 126614 A velocities reveals a strong periodicity near 3.4 yr. This periodicity closely matches the period of the best-fit, single-planet Keplerian model, which was found after a thorough search of the Keplerian parameters. Our model of a single planet plus a linear velocity trend has a distinctive staircase-like appearance (Figure 4) and the following best-fit parameters: $P = 3.41 \pm 0.05$ yr, $e = 0.41 \pm 0.10$, $K = 7.3 \pm 0.7$ m s^{-1}, and $dv/dt = 16.2 \pm 0.2$ m s^{-1} yr^{-1}, implying a planet of minimum mass $M \sin i = 0.38\ M_{Jup}$ orbiting with semimajor axis $a = 2.35$ AU. The full set of orbital parameters is listed in Table 3. The time series velocities (with trend subtracted) are plotted with the Keplerian model in Figure 5.

Table 5
Radial Velocities of HD 126614 A

JD–2440000	Radial Velocity (m s^{-1})	Uncertainty (m s^{-1})	Telescope
11200.13355	−175.78	1.26	K
11311.92294	−169.56	2.17	K
11342.85107	−155.44	1.47	K
11370.81727	−151.70	1.44	K
11373.83647	−146.70	1.77	K
11552.15999	−135.05	1.28	K
11553.16885	−136.56	1.34	K
11581.17426	−134.75	1.26	K
11583.06953	−140.19	1.44	K
11585.12509	−138.05	1.07	K
11586.03518	−134.02	1.14	K
11680.01873	−141.32	1.54	K
11982.14743	−126.57	1.45	K
12003.94759	−117.29	1.48	K
12005.13470	−118.83	1.38	K
12065.93845	−123.18	1.49	K
12096.76464	−116.69	1.78	K
12128.75811	−119.29	1.23	K
12335.07744	−112.03	1.39	K
12363.08412	−108.95	1.52	K
12389.99741	−110.09	1.77	K
12445.84007	−107.11	1.37	K
12683.05902	−82.87	1.34	K
12711.99652	−81.84	1.40	K
12776.95616	−76.98	1.47	K
12849.80405	−78.59	1.51	K
13015.15707	−70.77	1.29	K
13016.16478	−69.55	1.20	K
13017.15230	−70.34	1.25	K
13179.83922	−66.55	1.47	K
13425.13398	−57.71	1.18	K
13777.11170	−41.41	1.02	K
13838.01968	−39.62	1.62	K
14131.15530	−15.75	1.24	K
14246.94875	−18.96	0.93	K
14247.94129	−18.73	1.21	K
14248.90277	−18.55	1.16	K
14251.83500	−23.10	1.13	K
14255.78231	−20.33	0.87	K
14277.75659	−19.17	1.13	K
14278.76238	−18.63	1.22	K
14285.77622	−9.74	1.28	K
14294.83121	−18.26	1.19	K
14300.80378	−16.35	1.15	K
14493.17109	−9.46	1.12	K
14549.01403	−10.28	1.26	K
14639.85723	−11.05	1.25	K
14839.12869	−1.44	0.87	K
14865.17003	−3.63	1.66	K
14866.08003	−2.67	0.91	K
14927.91558	−3.71	1.42	K
14929.09501	−3.22	1.31	K
14930.03891	−2.54	1.15	K
14964.02038	−2.01	0.73	K
14983.79390	1.65	1.23	K
14984.84861	4.14	1.19	K
14985.95010	2.85	1.38	K
14986.93908	7.48	1.23	K
14987.94064	4.43	1.30	K
14988.95513	1.50	1.28	K
15014.82834	3.02	1.24	K
15015.83799	−1.02	1.25	K
15016.88768	0.91	1.07	K
15041.84683	4.80	1.33	K
15042.87063	8.59	1.45	K

Table 5
(Continued)

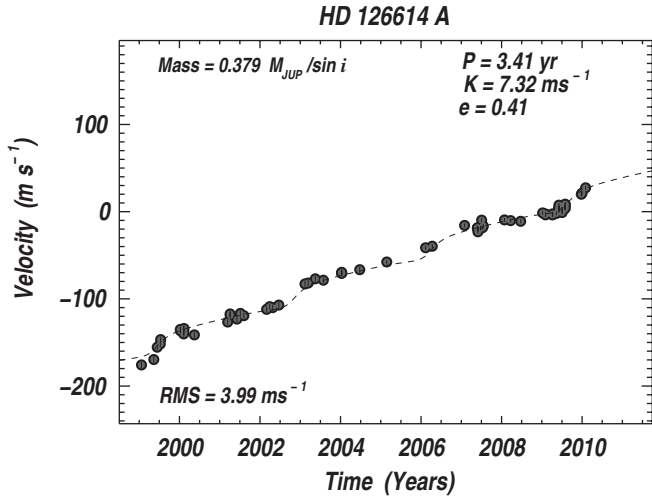| JD–2440000	Radial Velocity (m s^{-1})	Uncertainty (m s^{-1})	Telescope
15043.81939	3.67	1.33	K
15044.79615	7.78	1.40	K
15190.15992	19.99	1.34	K
15197.15781	21.27	1.23	K
15229.04986	27.36	1.19	K

HD 126614 A

Figure 4. Measured velocity vs. time for HD 126614 A (filled circles) and best-fit Keplerian model (dashed line). The strong linear trend of $dv/dt = 16.2$ m s^{-1} yr^{-1} is clearly seen. The error bars that represent the quadrature sum of measurement uncertainties and jitter are not visible on this scale. These data are plotted again with the linear trend removed in Figure 5.

This model of a single planet plus linear trend has rms velocity residuals of 3.99 m s^{-1} and $\chi_\nu = 1.42$, implying an adequate fit. We computed an FAP for the single-planet model using the $\Delta\chi^2$ statistic, as described in Section 4.3. We found that no scrambled data set had a larger value for $\Delta\chi^2$ than for the measured velocities, implying an FAP of less than $\sim$0.001 for this scenario.

6.4. Source of Linear RV Trend

The significant linear trend of 16.2 m s^{-1} yr^{-1} is likely due to a long-period stellar or planetary companion. We tried fitting the observed velocities with a two-planet model, using the Keplerian parameters of HD 126614 Ab and an outer planet with a wide variety of long periods as initial guesses. We were unable to find any two-planet models that improved χ_ν with statistical significance. Put another way, with a time baseline of 10 yr we do not detect curvature in the residuals to the one-planet model.

We also considered NLTT 37349 (2MASS J14264583-0510194) as the companion responsible for the observed acceleration. Gould & Chanamé (2004) identified this object as a common proper-motion partner to HD 126614 A with a sky-projected separation of 42″. The observed photometric properties of this object are $M_V = 12.02$, $V = 16.19$, and $V - J = 4.00$. Presumably NLTT 37349 has the same parallax (13.8 mas) and distance (72.4 pc) as HD 126614 A. Taken together, these properties are consistent with being an M dwarf, roughly M4, implying a mass of $m \sim 0.2\ M_\odot$. To compute the approximate gravitational influence of NLTT 37349, we assume that the line of sight separation between HD 126614 A and
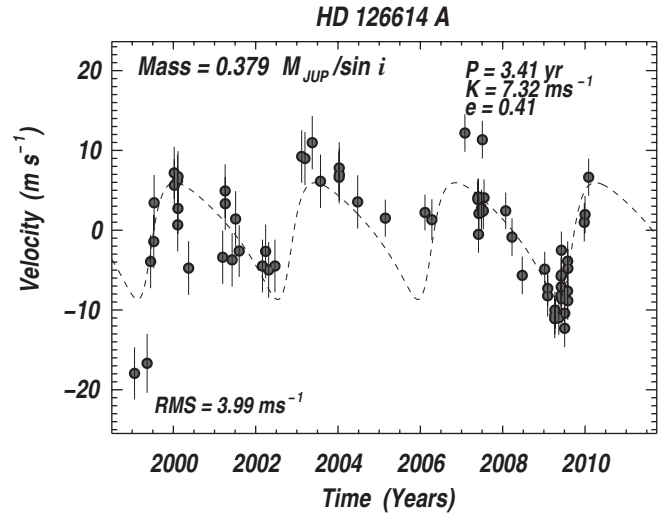
HD 126614 A

Figure 5. Same measured velocities (filled circles) and single planet Keplerian model (dashed line) for HD 126614 A as plotted in Figure 4, except the linear trend was subtracted before plotting.

NLTT 37349 is comparable to their physical separation in the sky plane, $r_{\rm sep} \sim 3000$ AU. The acceleration predicted by this model, $\dot{v}_r \sim Gm/r_{\rm sep}^2 = 0.004$ m s^{-1} yr^{-1}, is much too small to account for the observed acceleration of 16.2 m s^{-1} yr^{-1}. Thus, NLTT 37349 is not the source of the observed linear velocity trend.

Secular acceleration is a potential cause of a linear velocity trend, especially for stars with significant proper motion (such as HD 126614 A). While our standard velocity pipeline removed this effect from the velocities reported Table 5, it is reassuring to confirm that the calculated secular acceleration is inconsistent with the observed velocity trend. (The pipeline also removed the motion of Keck Observatory about the barycenter of the Solar System.) As discussed in Kürster et al. (2003) and Wright & Howard (2009), a star's proper motion will cause the the radial component of its space velocity vector to change with position on the sky, resulting a secular acceleration of $\dot{v}_r = D\mu^2$ (to first order), where v_r is the bulk RV of the star, D is the star's distance, and μ is the total proper motion in radians per unit time. For the most extreme cases of nearby stars with significant proper motion, $\dot{v}_r$ can be as high as a few m s^{-1} yr^{-1}. For HD 126614 A, we find $\dot{v}_r \sim 0.1$ m s^{-1} yr^{-1}, ruling out secular acceleration as the cause of the observed 16.2 m s^{-1} yr^{-1} trend.

6.5. AO Observations

Having ruled out the above reasons for the linear RV trend, we considered a stellar companion close enough to HD 126614 A to have been missed by prior imaging surveys. To search for such a companion, we obtained direct imaging of HD 126614 A in J, H, and K-short (K_s) bands on the Hale 200″ Telescope at Palomar Observatory on 2009 April 13 using the facility AO imager PHARO (Hayward et al. 2001). In each band, we co-added approximately one-fifty 431 ms exposures. As expected, the AO correction was best in K_s band, translating into the smallest errors. A nearby faint companion $\sim$500 mas to the Northeast of HD 126614 A was identified in each band by visual inspection (Figure 6). We constructed an empirical point-spread function (PSF) in each band from images of a calibrator, and images were fit with a two-PSF model. Parameter errors were calculated using the curvature of the χ^2 surface, and for consistency, the error in contrast ratio compared to the percent
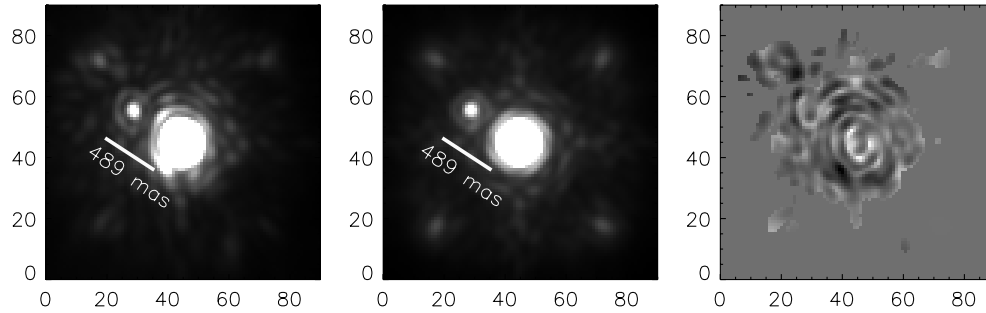
Figure 6. Direct observations with adaptive optics of HD 126614 A and HD 126614 B taken with the PHARO imager on Hale 200″ Telescope at Palomar Observatory. The three panels show K_s-band images of the target image (left), the best two-PSF fit (center), and fit residuals (right). Each image is oriented North-up and East-left. The fainter star, HD 126614 B, is clearly detected to the Northeast of the brighter target star, HD 126614 A. The vertical and horizontal axes of each image are labeled with detector pixels (the plate scale is 25.2 mas pixel^{-1}). The image gray scale has been chosen to highlight the companion, Airy rings, and diffraction spikes; the residuals (right panel) have been stretched by a factor of 150. The full width half-maximum of the AO-corrected PSF was ∼100 mas in each band (with Strehl ratios of 30% in K_s band and 10% in J band).

Table 6
Summary of AO Imaging Observations and Isochrone Analysis of HD 126614 B

	HD 126614 B				Gl 661 B	Padova Model
Filter	Separation (mas)	Pos. Angle (deg)	Cont. Ratio	M_{JHK} (mag)	M_{JHK} (mag)	HD 126614 B Mass ($M_\odot$)
J	498.7 ± 6.1	57.2 ± 0.9	45.3 ± 4.1	7.42	7.46	0.336 ± 0.015
H	487.1 ± 3.3	56.1 ± 0.6	38.8 ± 1.8	6.97	6.97	0.307 ± 0.007
K_s	488.5 ± 2.4	56.0 ± 0.3	35.0 ± 1.1	6.75	6.72	0.308 ± 0.005
Combined	489.0 ± 1.9	56.1 ± 0.3				0.324 ± 0.004

Notes. The absolute *JHK* magnitudes of HD 126614 B are derived from the measured contrast ratios, 2MASS photometry, and the Hipparcos parallax of HD 126614 A. The *J*-band results may be complicated by the presence of a diffraction spot near the position of the secondary. The uncertainties listed are based solely on the uncertainties in the contrast ratios. Accounting for all uncertainties, we estimate the combined mass to be accurate to perhaps 10%. For comparison, we show the absolute *JHK* magnitudes of Gl 661 B, with $M_V = 11.3$. This star was first identified in Reid & Gizis (1997) by speckle interferometry; we use updated photometry from Reid & Hawley (2005).

flux of the fit residuals. Combining the astrometric fits in all bands, we find a projected separation of 489.0 ± 1.9 mas at a position angle of 56.1 ± 0.3 deg.

We are unaware of a previous detection of this faint companion to HD 126614 A, which we name HD 126614 B. We summarize the astrometric and photometric results of the AO observations and the inferred properties of HD 126614 B in Table 6.

HD 126614 A and HD 126614 B are unresolved in the spectroscopic and photometric observations described in previous sub-sections. We estimate the amount of *V*-band contamination from HD 126614 B in these observations using three methods: model isochrones, observations of a similar star, and an empirical calibration employing metallicity effects.

First, we interpolated the log(age) = 9.1, $Z = 0.070$ (corresponding very nearly to [Fe/H] = +0.56) Padova isochrones (Girardi et al. 2000) at these absolute NIR magnitudes. These interpolations yield mass estimates for HD 126614 B (Table 6), the average of which is 0.324 ± 0.004 $M_\odot$, making HD 126614 B an M dwarf. The weighted average *V*-band magnitude implied by these measurements is $M_V = 10.65 ± 0.03$.

Second, we find that the M dwarf Gl 661 B has nearly identical NIR absolute magnitudes to HD 126614 B (Table 6; Reid & Hawley 2005). Nonetheless, its absolute V magnitude is in severe disagreement with the $Z = 0.070$ isochrones (and in even worse agreement with the solar metallicity isochrones). This suggests that the Padova isochrones significantly overestimate the *V*-band flux of M dwarfs. We thus consider the isochrone V magnitudes to be unreliable.

Finally, we have applied the M dwarf photometric calibration of Johnson & Apps (2009) to the absolute K_s magnitude derived from the AO photometry. This empirical calibration is based on G–M binaries with well-measured metallicities (from LTE spectral synthesis analysis of the primary) and K_s-band magnitudes of both components. Johnson & Apps find that a star with [Fe/H] = +0.56 and $M_{K_s} = 6.75$ should have $M_V = 12.2$. This estimate, which we feel is the most robust of the three we have performed, implies $V = 16.5$ and therefore negligible contamination in our optical spectra ($\Delta V = 7.8$, < 0.1% contamination).

Knowledge of the mass of HD 126614 B from the isochrones combined with the observed RV trend of HD 126614 A allows us to constrain the true physical separation between the stars. Let θ be the angle between the line of sight to the primary and the line connecting the primary to the secondary, such that the secondary is behind the primary when $\theta = 0$. The observed RV trend (the instantaneous acceleration along the line of sight) is related to θ, the mass of the secondary M_B, and the true physical separation r_{AB} by

$$\dot{v}_A = \frac{GM_B}{r_{AB}^2} \cos\theta, \qquad (1)$$

where r_{AB} is related to the apparent angular separation ρ_{AB} through

$$\left(\frac{r_{AB}}{AU}\right) \sin\theta = \frac{\rho_{AB}}{\pi_A} \qquad (2)$$

and π_A, the Hipparcos parallax of HD 126614 A. Given the observed radial acceleration of 16.2 m s^{-1} yr^{-1} and the best

separation and mass from Table 6, there are two solutions for the implied physical separation between the stars: $r_{AB} = 40^{+7}_{-4}$ and 50^{+2}_{-3} AU (where the uncertainty is dominated by the uncertainty in the parallax), which we can crudely combine as 45^{+7}_{-9} AU with the caveat that the probability distribution function is highly non-Gaussian.

Holman & Wiegert (1999) studied the dynamical stability of planetary orbits in binary systems. In the terms of that work, we find the mass ratio of the binary system to be $\mu = 0.22$, at the edge of Hill's Regime. Holman & Wiegert find that for a binary in a circular orbit, planets in S-type orbits of semimajor axis a_b are generally stable when secondary stars orbit with semimajor axes $a_B > a_b/0.38$. For our system, this yields $a_B > 6.2$ AU, consistent with our AO astrometry. Indeed, the HD 126614 system unconditionally passes this weak test for stability for $e_B < 0.6$; beyond this regime more detailed knowledge of the binary orbit is required for further analysis.

Pfahl & Muterspaugh (2006) discuss the prevalence of planets in binary systems such as HD 126614. They note that the literature contains a few planet detections in systems separated by ∼20 AU, the most similar to HD 126614 being HD 196885 (Fischer et al. 2009). Thus, HD 126614 Ab appears to be in a stable orbit in a binary system that is not atypical, even among systems with detected planets.

6.6. Planetary Interpretation

The identification of HD 126614 as a stellar binary with a separation of ∼0″.5 (unresolved by Keck/HIRES) raises the question of the origin of the periodic RV signal described in Section 6.3. We investigated the possibility that the RV variation was the result of distortions in the spectral line profiles due to contamination of the HD 126614 A spectrum by the much fainter HD 126614 B spectrum modulated by an orbital companion of its own. We present multiple lines of reasoning to argue against this alternative explanation and in favor of the Jovian-mass planet orbiting HD 126614 A described in Section 6.3.

From the AO observations in *JHK* bands, we estimated the *V*-band flux of HD 126614 B in several ways with the most reliable method giving a flux ratio (A/B) of 7.8 mag. Thus, in the iodine region of the spectrum, the lines from HD 126614 B are fainter by a factor of ∼10^3. To produce a Doppler signal with $K = 7$ m s^{-1} when diluted by HD 126614 A, the signal from HD 126614 B would have an amplitude of approximately $K = 7$ km s^{-1} (implying a companion orbiting HD 126614 B with mass 0.25 $M_{\odot}$, an M dwarf). Yet, the stellar lines of HD 126614 A, with $v \sin i = 1.52$ km s^{-1}, are narrower than the amplitude of the hypothetical $K = 7$ km s^{-1} Doppler signal. Thus, the stellar line profiles of HD 126614 A and HD 126614 B would not be blended, but separated from each other for most of the 3.41 yr orbit. This inconsistency casts serious doubt on the blend scenario as an explanation for the observed RV variation.

Nevertheless, we investigated the blend scenario further with a spectral line bisector span test (Torres et al. 2005; Queloz et al. 2001). We chose a region of the spectrum (6795–6865 Å) to the red of the iodine region for increased sensitivity to the spectral features of HD 126614 B (an M dwarf) and a lack of telluric contamination. We cross-correlated each post-upgrade Keck spectrum against the solar spectrum using the National Solar Observatory solar atlas (Kurucz et al. 1984). From this representation of the average spectral line profile we computed the bisectors of the cross-correlation peak, and as a measure of the line asymmetry we calculated the "bisector span" as the

velocity difference between points selected near the top and bottom of the cross-correlation peak. If the velocities were the result of a blend, we would expect the line bisectors to vary in phase with the 3.41 yr period with an amplitude similar to $K = 7$ m s^{-1}. Instead, we find no significant correlation between the bisector spans and the RVs after subtracting the 16.2 m s^{-1} yr^{-1} trend. The Pearson linear correlation coefficient between these two quantities, $r = -0.28$, demonstrates the lack of correlation. We conclude that the velocity variations are real and that the star is orbited by a Jovian planet.

7. HD 13931

7.1. Stellar Characteristics

HD 13931 (= HIP 10626) is spectral type G0 V, with $V = 7.61$, $B - V = 0.64$, and $M_V = 4.32$, placing it ∼0.4 mag above the main sequence. It is chromospherically quiet with $S_{HK} = 0.16$ and $\log R'_{HK} = -4.99$ (Isaacson 2009), implying a rotation period of ∼26 days (Noyes et al. 1984). Valenti & Fischer (2005) measured an approximately solar metallicity of [Fe/H] = +0.03 using SME. Its placement above the main sequence and low chromospheric activity are consistent with an old, quiescent star of age 6.4–10.4 Gyr.

7.2. Photometry from Fairborn Observatory

We have 181 photometric observations of HD 13931 over two consecutive observing seasons. Periodogram analyses found no significant periodicity over the range 1–100 days. The short-term standard deviations of the target and comparison stars (Table 2) provide an upper limit of 0.0016 mag for night-to-night variability. The long-term standard deviations suggest intrinsic low-level variability in HD 13931, but additional observations are needed to confirm it.

7.3. Doppler Observations and Keplerian Fit

We monitored the RV of HD 13931 at Keck for the past 12 yr. Table 7 gives the Julian Dates of the observations, the measured (relative) radial velocities, and the associated measurement uncertainties (excluding jitter). The 39 velocities listed in Table 7 have an rms of 15.1 m s^{-1}. These velocities are plotted as a time series in Figure 7 along with the best-fit Keplerian model.

A long period signal that has completed approximately one cycle is clearly seen in the velocities plotted in Figure 7. After trying a wide variety of trial periods, we found the best-fit, single-planet Keplerian model with $P = 11.5 \pm 1.1$ yr, $e = 0.02 \pm 0.08$, and $K = 23.3 \pm 2.9$ m s^{-1}, implying a planet of minimum mass $M \sin i = 1.88$ M_{Jup} orbiting with semimajor axis $a = 5.15$ AU. Note that the orbit is consistent with being circular. The full set of orbital parameters is listed in Table 3. This model, with $\chi_\nu = 1.01$ and 3.31 m s^{-1} rms velocity residuals, is an excellent fit to the data. Under the assumption of a one-planet model, we observed three RV extrema with Keck that strongly constrain the orbital parameters.

8. GL 179

8.1. Stellar Characteristics

Gl 179 (= HIP 22627) is spectral type M3.5 V, with $V = 11.96$, $B - V = 1.59$, and $M_V = 11.5$, placing it ∼0.3 mag above the main sequence. It is chromospherically active with $S_{HK} = 0.96$ (Isaacson 2009). Valenti & Fischer (2005) did not calculate
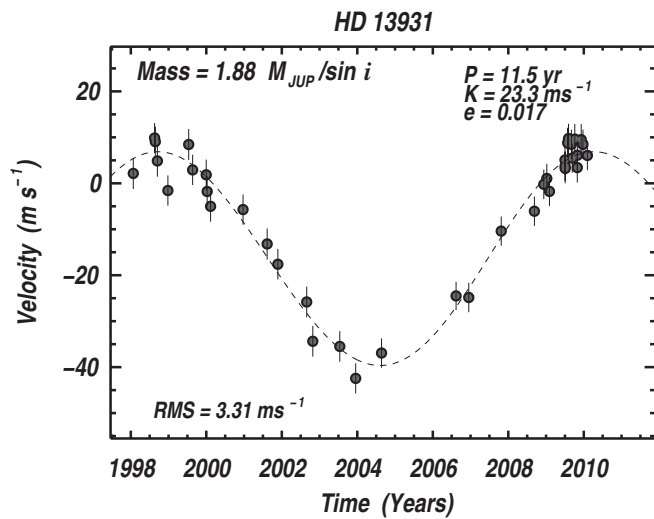
HD 13931

Figure 7. Measured velocity vs. time for HD 13191 (filled circles) with the associated best-fit Keplerian model (dashed line). The error bars show the quadrature sum of measurement uncertainties and jitter.

Table 7
Radial Velocities of HD 13931

JD–2440000	Radial Velocity (m s^{-1})	Uncertainty (m s^{-1})	Telescope
10837.81679	2.15	1.59	K
11044.11226	9.86	1.26	K
11051.05061	9.06	1.27	K
11071.05334	4.87	1.66	K
11172.82617	−1.57	1.34	K
11374.13082	8.45	1.55	K
11412.08069	2.92	1.37	K
11543.80646	1.85	1.38	K
11552.79058	−1.78	1.56	K
11585.71983	−5.01	1.46	K
11899.88418	−5.72	1.33	K
12133.12439	−13.19	1.56	K
12236.81830	−17.61	1.44	K
12515.95280	−25.82	1.44	K
12574.90240	−34.38	1.45	K
12836.11950	−35.49	1.45	K
12989.72665	−42.44	1.35	K
13240.00935	−36.93	1.11	K
13961.11345	−24.51	0.64	K
14083.90911	−24.85	1.11	K
14397.92588	−10.40	1.05	K
14719.07441	−6.08	1.09	K
14809.83689	−0.23	1.14	K
14838.92165	1.05	1.08	K
14864.76650	−1.77	1.09	K
15015.10431	5.07	1.12	K
15016.10240	3.72	1.11	K
15017.10744	3.23	1.19	K
15042.12880	8.88	1.19	K
15044.13700	8.69	1.14	K
15049.04212	9.74	1.17	K
15077.13808	8.48	1.05	K
15085.13348	5.48	1.02	K
15109.99945	9.62	1.38	K
15133.95126	3.42	1.25	K
15134.91132	6.11	1.22	K
15171.97729	9.50	1.59	K
15188.89679	8.46	1.18	K
15231.78501	6.06	1.12	K

Table 8
Radial Velocities of Gl 179

JD–2440000	Radial Velocity (m s^{-1})	Uncertainty (m s^{-1})	Telescope
11580.83131	38.12	4.05	K
11882.88790	37.65	4.87	K
11901.00250	30.81	5.13	K
12235.84867	54.65	6.14	K
12536.08795	4.11	4.50	K
12572.99093	28.53	5.14	K
12573.95028	17.59	4.52	K
12575.04686	5.25	4.48	K
12575.99081	9.58	5.42	K
12898.11579	−8.75	4.24	K
13014.81847	−7.72	4.53	K
13015.83165	−16.60	4.26	K
13016.83228	−29.20	3.72	K
13297.85507	−1.09	10.33	H
13299.84862	14.31	5.54	H
13302.97472	2.28	1.93	K
13314.80754	8.21	4.36	H
13340.72400	2.54	5.09	H
13631.92988	10.84	15.59	H
13644.90017	25.11	12.87	H
13686.92171	9.61	6.64	H
13719.83142	28.29	12.94	H
13984.08891	32.57	2.23	K
14130.85314	35.38	2.51	K
14397.93848	39.52	2.15	K
14411.93712	17.96	14.13	H
14771.80303	22.44	4.48	H
14778.99120	21.36	2.43	K
14790.99549	13.51	2.39	K
14807.91708	12.78	2.17	K
14838.99126	19.51	1.76	K
14846.95665	11.56	2.70	K
14864.95689	14.55	2.42	K
14928.73249	6.67	2.03	K
14929.72575	4.21	2.64	K
14934.73136	−8.63	2.88	K
15077.10989	3.80	1.99	K
15084.94943	−1.33	7.22	H
15170.78663	−5.85	1.68	K
15174.09252	−14.84	2.27	K
15175.70740	−15.10	8.34	H
15180.83537	−32.31	5.00	H
15187.83709	−19.44	2.46	K
15206.77569	−3.89	4.39	H

stellar parameters using SME for Gl 179 because of its late spectral type. Similarly, the Noyes et al. (1984) calibration of stellar rotation does not apply for $B − V > 1.4$. Johnson & Apps (2009) find a high metallicity of [Fe/H] $= 0.30 ± 0.10$ for Gl 179 based on its absolute K-band magnitude, M_K, and $V − K$ color.

8.2. Photometry from Fairborn Observatory

We have not made photometric observations of Gl 179 from the APTs because at $V = 11.96$ the star is too faint.

8.3. Doppler Observations and Keplerian Fit

We monitored the RV of Gl 179 at Keck for the past 10 yr and at the HET for the past 5 yr. Table 8 gives the Julian Dates of the observations, the measured (relative) radial velocities, the associated measurement uncertainties (excluding jitter), and
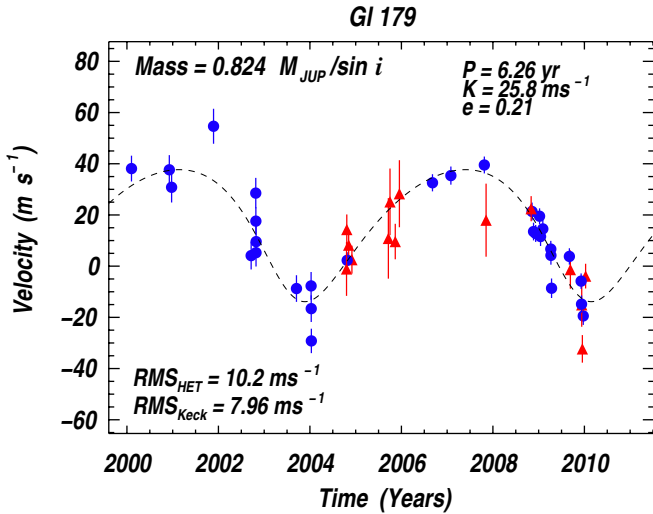
Figure 8. Measured velocity vs. time for Gl 179 (filled circles) with the associated best-fit Keplerian model (dashed line). Filled blue circles represent measurements from Keck, while filled red triangles represent HET measurements. The error bars show the quadrature sum of measurement uncertainties and jitter.

the telescope used. The 44 velocities listed in Table 8 have an rms of 19.7 m s^{-1}. Because Gl 179 is a faint M dwarf, the measurements have lower signal-to-noise ratios and larger uncertainties compared to the other stars in this paper. The measured velocities are plotted as a time series in Figure 8 along with the best-fit Keplerian model.

After trying a wide variety of trial orbital periods, we find the best-fit, single-planet Keplerian model has $P = 6.26 \pm 0.16$ yr, $e = 0.21 \pm 0.08$, and $K = 25.8 \pm 2.2$ m s^{-1}, implying a planet of minimum mass $M \sin i = 0.82 M_{\rm Jup}$ orbiting with semimajor axis $a = 2.41$ AU. The full set of orbital parameters is listed in Table 3. We allowed for floating offsets between the HET RVs, the pre-upgrade Keck RVs, and the post-upgrade RVs when fitting the data.

Note that the planet is clearly detected in the Keck RVs alone, but the HET measurements are crucial for the precise determination of orbital parameters, especially eccentricity and minimum mass. This single planet model, with $\chi_\nu = 1.78$ and 9.51 m s^{-1} rms velocity residuals, is a statistically significant improvement over a model with no planets. However, the relatively large value of χ_ν implies that either additional planets remain undetected in the system or we have underestimated the measurement uncertainties or jitter. We will continue to observe Gl 179 to search for additional planets.

9. DISCUSSION

We present the detection of four new extrasolar planets. These planets add to the statistical properties of giant planets in long-period orbits near the ice line. Long observational time baselines (10–12 yr) were necessary to accurately measure the high-eccentricity, low-amplitude signals of HD 34445 b and HD 126614 Ab, as well as the intermediate-amplitude, but long-period signals of HD 13931 b and Gl 179 b.

HD 34445 b is a massive planet ($M \sin i = 0.79 M_{\rm Jup}$) in a mildly eccentric ($e = 0.27$), long-period ($P = 2.87$ yr) orbit around an old G0 dwarf. We clearly detect this planet in the Keck and HET data sets individually, and their combination allows for more precise orbit determination. The relatively large

residuals to the one-planet fit (rms = 6–8 m s^{-1}) hint at a second, unresolved planet in the system. Underestimated jitter would also explain the large residuals, but we deem this explanation less likely given the metallicity, color, and modest evolution of HD 34445.

HD 126614 Ab is a massive planet ($M \sin i = 0.38 M_{\rm Jup}$) in a long-period ($P = 3.41$ yr), eccentric ($e = 0.41$) orbit around an extremely metal-rich star. At [Fe/H] = +0.56 ±0.04, HD 126614 A has the highest metallicity of the 1040 stars in the SPOCS catalog (Valenti & Fischer 2005). It also has the highest [Fe/H] of the ∼250 stars with known planets and measured metallicities. We confirmed the high metallicity of HD 126614 A by running a separate iodine-free HIRES spectrum through the same SME pipeline used for the SPOCS catalog. We found [Fe/H] = +0.51 ±0.04, consistent with the SPOCS catalog value. Other authors also find an extremely high metallicity, including Castro et al. (1997) and Cenarro et al. (2007), who both find [Fe/H] = +0.55. These measurements, along with the detection of HD 126614 Ab, add statistical weight to the strong positive correlation between giant planet occurrence and metallicity (Fischer & Valenti 2005). Indeed, HD 126614 A has been part of the planet-metallicity correlation story for some time. In an early paper discussing the host star properties of some of the first extrasolar planets, Gonzalez et al. (1999) suggested that two bright, high-metallicity stars, namely HD 99109 and HD 126614, should be searched for Doppler variations. HD 99109 is known to host a planet with minimum mass $M \sin i = 0.5 M_{\rm Jup}$ and orbital period $P = 1.2$ yr (Butler et al. 2006), and HD 126614 A now joins the list of high-metallicity stars with planets.

In addition to the planet orbiting HD 126614 A, we detected a faint M dwarf companion using AO and the PHARO camera at Palomar Observatory. This previously undiscovered star, HD 126614 B, has an estimated mass of 0.32 $M_\odot$ and is separated from HD 126614 A by 489 ± 1.9 mas at position angle 56.1 ± 0.3 deg. This corresponds to a projected separation of 33 AU.

HD 13931 b is reminiscent of Jupiter in orbital period ($P = 11.5$ yr), eccentricity ($e = 0.02$), and to a lesser extent mass ($M \sin i = 1.88 M_{\rm Jup}$). The host star, HD 13931, is also similar to the Sun in mass ($M_\star = 1.02 M_\odot$) and metallicity ([Fe/H] = +0.03). HD 13931 b is one of only four known RV-detected planets with orbital periods longer than 10 yr. The other such planets—55 Cnc d (Fischer et al. 2008), HD 217107 c (Vogt et al. 2005; Wright et al. 2009) and HD 187123 c (Wright et al. 2007, 2009)—are all in multi-planet systems.

Gl 179 b is a Jovian-mass ($M \sin i = 0.82 M_{\rm Jup}$) planet in a long-period ($P = 6.3$ yr) orbit. The host star, Gl 179, is one of only ∼10 M dwarfs currently known to host a planet and is among the faintest ($V = 11.96$) stars with a planet discovered by RV measurements. This planet is detected in the Keck velocities alone, but without the HET measurements, the orbital parameters, especially eccentricity and minimum mass, would be determined more poorly.

We note with interest that Gl 179 is an almost identical twin to Gl 876, an M dwarf known to host two Jovian planets locked in resonant orbits and a super-Earth in a $P = 1.9$ day orbit (Marcy et al. 2001; Rivera et al. 2005). The stars are similar in effective temperature, mass, and age, as traced respectively by $V - K$ color (5.00 for Gl 179 and 5.15 for Gl 876), M_K (6.49 for Gl 179 and 6.67 for Gl 876), and $S_{\rm HK}$ (0.96 for Gl 179 and 1.02 for Gl 876). The high metallicity of Gl 179 is also strikingly similar to the metallicity of Gl 876. Johnson & Apps (2009) estimate

[Fe/H] = +0.3 and +0.37 for Gl 179 and Gl 876, respectively. Based on their analysis of M dwarfs with planets, Johnson & Apps find that the planet-metallicity correlation holds for stars at the bottom of the main sequence. Gl 179 and its planet add statistical weight to this finding.

The planet-bearing stars presented here are good candidates for follow-up astrometric and direct imaging observations. The astrometric perturbations from these planets on their host stars (10's to 100's of μas) will be quite detectable with the expected sub-μas sensitivity of NASA's SIM or its proposed variants. Direct detection is also plausible using coronagraphs/ interferometers on space-borne and next-generation ground-based observatories, including GPI and SPHERE. HD 13931 b may be the best candidate with a maximum projected angular separation of 120 mas. Indeed, SIM observations of HD 13931, even over a fraction of the orbital period (SIM has a planned mission duration of five years), combined with the RV measurements presented here, would completely determine the three-dimensional orbit, giving accurate predictions of the best times for direct imaging observations.

REFERENCES

Alibert, Y., Mordasini, C., Benz, W., & Winisdoerffer, C. 2005, A&A, 434, 343
Beichman, C. A., Fridlund, M., Traub, W. A., Stapelfeldt, K. R., Quirrenbach, A., & Seager, S. 2007, in Protostars and Planets V, ed. B. Reipurth, D. Jewitt, & K. Keil (Tucson, AZ: Univ. Arizona Press), 915
Benz, W., Mordasini, C., Alibert, Y., & Naef, D. 2008, Phys. Scr. T, 130, 014022
Bessell, M. S. 1995, in Proc. ESO, The Bottom of the Main Sequence–and Beyond, ed. C. G. Tinney (Berlin: Springer), 123
Butler, R. P., Marcy, G. W., Williams, E., McCarthy, C., Dosanjh, P., & Vogt, S. S. 1996, PASP, 108, 500
Butler, R. P., et al. 2006, ApJ, 646, 505
Castro, S., Rich, R. M., Grenon, M., Barbuy, B., & McCarthy, J. K. 1997, AJ, 114, 376
Cenarro, A. J., et al. 2007, MNRAS, 374, 664
Cochran, W. D., et al. 2004, ApJ, 611, L133
Cumming, A., Butler, R. P., Marcy, G. W., Vogt, S. S., Wright, J. T., & Fischer, D. A. 2008, PASP, 120, 531
Delfosse, X., Forveille, T., Ségransan, D., Beuzit, J.-L., Udry, S., Perrier, C., & Mayor, M. 2000, A&A, 364, 217
Dodson-Robinson, S. E., Bodenheimer, P., Laughlin, G., Willacy, K., Turner, N. J., & Beichman, C. A. 2008, ApJ, 688, L99
Endl, M., Cochran, W. D., Tull, R. G., & MacQueen, P. J. 2003, AJ, 126, 3099
Endl, M., Kürster, M., & Els, S. 2000, A&A, 362, 585
Fischer, D. A., & Valenti, J. 2005, ApJ, 622, 1102
Fischer, D. A., et al. 2008, ApJ, 675, 790
Fischer, D. A., et al. 2009, ApJ, 703, 1545
Ford, E. B., & Chiang, E. I. 2007, ApJ, 661, 602
Ford, E. B., & Rasio, F. A. 2008, ApJ, 686, 621
Girardi, L., Bressan, A., Bertelli, G., & Chiosi, C. 2000, A&AS, 141, 371
Gonzalez, G., Wallerstein, G., & Saar, S. H. 1999, ApJ, 511, L111
Gould, A., & Chanamé, J. 2004, ApJS, 150, 455
Hayward, T. L., Brandl, B., Pirger, B., Blacken, C., Gull, G. E., Schoenwald, J., & Houck, J. R. 2001, PASP, 113, 105
Henry, G. W. 1999, PASP, 111, 845
Henry, G. W., Fekel, F. C., & Hall, D. S. 1995, AJ, 110, 2926
Holman, M. J., & Wiegert, P. A. 1999, AJ, 117, 621
Howard, A. W., et al. 2009, ApJ, 696, 75
Ida, S., & Lin, D. N. C. 2008, ApJ, 685, 584
Isaacson, H. T. 2009, BAAS, 41, 206
Jansson, P. 1995, Deconvolution: With Applications in Spectroscopy (New York: Academic Press)
Johnson, J. A., & Apps, K. 2009, ApJ, 699, 933
Johnson, J. A., Butler, R. P., Marcy, G. W., Fischer, D. A., Vogt, S. S., Wright, J. T., & Peek, K. M. G. 2007a, ApJ, 670, 833
Johnson, J. A., et al. 2007b, ApJ, 665, 785
Jurić, M., & Tremaine, S. 2008, ApJ, 686, 603
Kaltenegger, L., Eiroa, C., & Fridlund, C. V. M. 2010, Ap&SS, 326, 233
Kaltenegger, L., Fridlund, M., & Karlsson, A. 2006, Ap&SS, 306, 147
Kürster, M., et al. 2003, A&A, 403, 1077
Kurucz, R. L., Furenlid, I., Brault, J., & Testerman, L. 1984, Solar Flux Atlas from 296 to 1300 nm (Sunspot, New Mexico: National Solar Observatory)
Lawson, P. R., et al. 2008, Proc. SPIE, 7013, 70132N-1
Lisse, C. M., Beichman, C. A., Bryden, G., & Wyatt, M. C. 2007, ApJ, 658, 584
Marcy, G. W., & Butler, R. P. 1992, PASP, 104, 270
Marcy, G. W., Butler, R. P., Fischer, D., Vogt, S. S., Lissauer, J. J., & Rivera, E. J. 2001, ApJ, 556, 296
Marcy, G. W., Butler, R. P., Vogt, S. S., Fischer, D. A., Henry, G. W., Laughlin, G., Wright, J. T., & Johnson, J. A. 2005, ApJ, 619, 570
Marcy, G. W., et al. 2008, Phys. Scr. T, 130, 014001
Mayor, M., & Udry, S. 2008, Phys. Scr. T, 130, 014010
Noyes, R. W., Hartmann, L. W., Baliunas, S. L., Duncan, D. K., & Vaughan, A. H. 1984, ApJ, 279, 763
Paulson, D. B., Saar, S. H., Cochran, W. D., & Henry, G. W. 2004, AJ, 127, 1644
Payne, M. J., Ford, E. B., Wyatt, M. C., & Booth, M. 2009, MNRAS, 393, 1219
Pfahl, E., & Muterspaugh, M. 2006, ApJ, 652, 1694
Queloz, D., et al. 2001, A&A, 379, 279
Ramsey, L. W., et al. 1998, Proc. SPIE, 3352, 34
Reid, I. N., & Gizis, J. E. 1997, AJ, 113, 2246
Reid, I. N., & Hawley, S. L. 2005, New Light on Dark Stars : Red Dwarfs, Low-mass Stars, Brown Dwarfs (2nd ed.; Chichester: Praxis Publishing Ltd)
Rice, W. K. M., & Armitage, P. J. 2005, ApJ, 630, 1107
Rivera, E. J., et al. 2005, ApJ, 634, 625
Saar, S. H., Butler, R. P., & Marcy, G. W. 1998, ApJ, 498, L153
Takeda, G., Ford, E. B., Sills, A., Rasio, F. A., Fischer, D. A., & Valenti, J. A. 2007, ApJS, 168, 297
Takeda, G., Ford, E. B., Sills, A., Rasio, F. A., Fischer, D. A., & Valenti, J. A. 2008, VizieR Online Data Catalog, 216, 80297
Thommes, E. W., Matsumura, S., & Rasio, F. A. 2008, Science, 321, 814
Torres, G., Konacki, M., Sasselov, D. D., & Jha, S. 2005, ApJ, 619, 558
Traub, W. A., et al. 2010, EAS Publication Series, Extrasolar Planets in Multi-body Systems: Theory and Observations, 42, 191
Trilling, D. E., Lunine, J. I., & Benz, W. 2002, A&A, 394, 241
Tull, R. G. 1998, Proc. SPIE, 3355, 387
Unwin, S. C., et al. 2008, PASP, 120, 38
Valenti, J. A., Butler, R. P., & Marcy, G. W. 1995, PASP, 107, 966
Valenti, J. A., & Fischer, D. A. 2005, ApJS, 159, 141
Valenti, J. A., & Piskunov, N. 1996, A&AS, 118, 595
van Leeuwen, F. 2007, A&A, 474, 653

Vogt, S. S., Butler, R. P., Marcy, G. W., Fischer, D. A., Henry, G. W., Laughlin, G., Wright, J. T., & Johnson, J. A. 2005, ApJ, 632, 638
Vogt, S. S., et al. 1994, Proc. SPIE, 2198, 362
Winn, J. N., Henry, G. W., Torres, G., & Holman, M. J. 2008, ApJ, 675, 1531
Wright, J. T. 2005, PASP, 117, 657
Wright, J. T., & Howard, A. W. 2009, ApJS, 182, 205
Wright, J. T., Marcy, G. W., Butler, R. P., & Vogt, S. S. 2004, ApJS, 152, 261
Wright, J. T., Marcy, G. W., Butler, R. P., Vogt, S. S., Henry, G. W., Isaacson, H., & Howard, A. W. 2008, ApJ, 683, L63
Wright, J. T., Upadhyay, S., Marcy, G. W., Fischer, D. A., Ford, E. B., & Johnson, J. A. 2009, ApJ, 693, 1084
Wright, J. T., et al. 2007, ApJ, 657, 533